Non-conventional positron source target simulations for the International Linear Collider

S. Geaney[†]
The University of Manchester, United Kingdom

Supervisors:
S. Riemann & F. Staufenbiel
Deutsches Elektronen-Synchrotron, Germany

DESY Summer Student Programme

August 2013

Abstract

The international linear collider (ILC) will be designed to collide electrons and positrons at high center of mass energies. The colliding leptons need to be polarised to experimentally test the accuracy of theoretically predicted left-right asymmetry cross-sections. Simulations for a Ti(6%)Al(4%)V alloy target, for the pair production of positrons, were carried out for two designs to observe the effects of a high energy photon beam on the alloy. This report discusses the simulated temperature distributions, structural deformation and bearing forces for one proposed positron target design that conforms to the specifications of the ILC technical design report.

[†]*E-mail:* shaun.geaney@student.manchester.ac.uk

Contents

1 Introduction

The experimental confirmation of a 'Higgs boson' like particle at the Large Hadron Collider (LHC) at CERN in 2013 was able to determine the mass of the particle to be approximately 126 GeV. Other quantum properties of the particle were also measured and appear to support the notion that this is the standard model Higgs boson [1].

This particle was observed through proton-proton collisions. The proton is a composite object consisting of three quarks and therefore the centre of mass energy is less precisely known. This makes resolving these hadronic events more difficult and involves the use of parton density functions to extrapolate back to a potential Higgs event.

However, by exploiting the point-like nature of leptons in high-energy collisions, it is possible to measure the centre of mass energy to a much higher precision. This negates the need of parton density functions in the event analysis. Hence, to further probe the properties of the Higgs boson, a linear collider has been proposed that will collide electrons and positrons together to explore properties of this particle.

1.1 International Linear Collider

The ILC is a proposed linear accelerator that will initially collide electrons and positrons at a centre of mass energy of 250 GeV to create a Higgs factory. Then to 350 GeV and 500 GeV for top quark centre of mass collisions and for new particle searches, respectively. The ILC can potentially be upgraded to 1 TeV centre of mass energy for further particle exploration. This will consist of two 12 km linacs containing superconducting cavities that will accelerate the leptons to the required energies [2].

The current design for the ILC is shown below in figure 1. It includes two complementary detectors that will be independently operated. This is to provide reliability of results from the ILC and cross-checkable discoveries for both detectors [3]. The design will have two damping rings for each of the electron and positron beams. These are to dampen any instability of the beams along their respective axes and to delay the beams for upstream accelerator sections if necessary. Two main linacs will accelerate each of the electron and positron beams from their injection energy of 15 GeV to 250 GeV. The beams will be accelerated by the cavities and will be cooled to an approximate temperature of 2 K, super-fluid helium temperatures. The design requires polarising electron and positron sources. The electron source will have greater than 80% polarisation from a laser illuminated photocathode in a DC gun. The polarised positron target is the focus of this report and is discussed in detail elsewhere in the report [4].

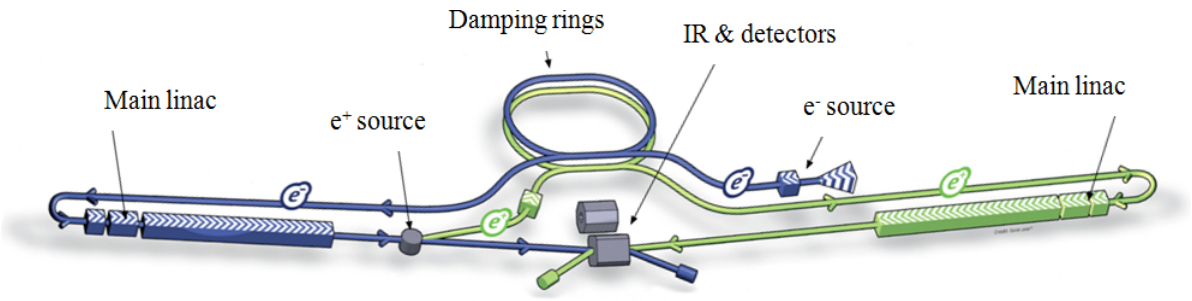

Figure 1: The current design for the International Linear Collider. The detectors overlap the interaction point of the two beams. The beams collide at a crossing angle to prevent the resulting particles from re-entering the beam channels [5].

1.2 Positron Source

Positrons will be created through photo-production as circularly polarised 10 - 30 MeV photons are incident upon a metal target. The positron source needs to have a collimator and target that can withstand the beam power and the deposited thermal energies. The source needs to also transport, with minimal beam loss, the bunches to the damping rings. Figure 2 shows a schematic of the positron source.

Pre-accelerated electrons from the main linac that are heading to the interaction point enter a helical undulator where they emit circularly polarised synchrotron radiation. The radiation is due to the transverse helical field created by helically wound superconducting magnets. The undulator will be approximately 150 m in length. Once the photons have been produced, the electrons will be deflected and directed to an electron dump. The photon beam is then collimated for 500 m before hitting the positron target. The target design is a rotating titanium alloy wheel, the specifics of two possible designs are discussed further in section 3. The target is designed to have a thickness of 0.4 radiation lengths (or 1.4 cm). The rotational velocity will be between 1,000 - 2,000 rpm and will receive a beam spot size of approximately 1.7 mm. The whole target structure will be kept in a vacuum enclosure of approximately 10^{-11} atm. The resultant positrons will then be focused with an Optical Matching Device (OMD) that generates a solenoidal magnetic field that increases the capture efficiency of the beams. The positron beam is then accelerated by an RF cavity and delivered to the damping rings [4].

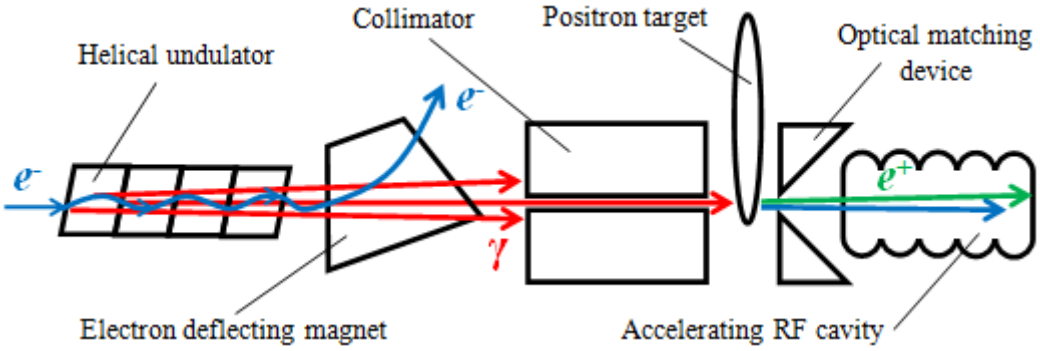

Figure 2: The positron source. Electrons enter a helical undulator to produce circularly polarised photons. The photons are collimated and then pair produce electrons and positrons.

2 Theory

2.1 Polarised Particles

The polarisation of both e^- e^+ beams is an upgradable possibility to the ILC. The importance of which is widely accepted. Some of the advantages of this choice of polarised beams are that background processes can be suppressed in weak interactions such as Z^0 production via WW fusion. The background suppression can be as high as a factor of two. Top couplings can also be used to measure the left-right asymmetry (A_{LR}) for the coupling of bosons to fermions. Due to the large mass of the top quark, it is near to the electroweak symmetry breaking scale, therefore making it an ideal candidate to explore the Higgs mechanism [6].

In the Standard Model (SM), the cross-section can be affected and altered by beam polarisation. The best example of this can be described in the framework of the colliding polarised beams producing a fermion-pair. The cross-section for such a process can be

written as

$$\begin{aligned}\sigma_{\mathcal{P}_{e^-}\mathcal{P}_{e^+}} = \frac{1}{4}[&(1-\mathcal{P}_{e^-})(1+\mathcal{P}_{e^+})\sigma_{LR} + (1+\mathcal{P}_{e^-})(1-\mathcal{P}_{e^+})\sigma_{RL} \\ &+(1-\mathcal{P}_{e^-})(1-\mathcal{P}_{e^+})\sigma_{LL} + (1+\mathcal{P}_{e^-})(1+\mathcal{P}_{e^+})\sigma_{RR}]\end{aligned} \tag{1}$$

where $\mathcal{P}_{e^-}$ and $\mathcal{P}_{e^+}$ denote the electron and positron polarisations, respectively. By convention, σ_{LR} represents the cross-section of a 100% left-handed polarised electron beam ($\mathcal{P}_{e^-} = -1$) and of a 100% right-handed polarised positron ($\mathcal{P}_{e^+} = 1$). The other remaining cross-sections are consequentially defined given this convention. Since two fermions annihilate and two other fermions are produced, an exchange of a spin-1 vector boson (γ or Z^0) is required. For spin conservation, the only possible interactions are for $J = 1$ and hence, σ_{RR} and σ_{LL} are zero in the SM. This is shown in table 1, along with combinations of the electron and positron helicities (± 1). This approach assumes that no other unknown particles contribute to the cross-sections and that any contribution from the Higgs is negligible [7].

$\hat{J}$	$e^- \longrightarrow \quad \longleftarrow e^+$	h_{e^-} & h_{e^+}	cross-section
1	$\Leftarrow\rightarrow \quad \leftarrow\Leftarrow$	$-1 \ +1$	σ_{LR}
1	$\Rightarrow\rightarrow \quad \leftarrow\Rightarrow$	$+1 \ -1$	σ_{RL}
0	$\Rightarrow\rightarrow \quad \leftarrow\Leftarrow$	$+1 \ +1$	σ_{RR}
0	$\Leftarrow\rightarrow \quad \leftarrow\Rightarrow$	$-1 \ -1$	σ_{LL}

Table 1: Every collision combination. In the second column, the single arrow represents the particles linear momentum whereas the double arrow represents the spin direction [7].

By defining the a left-right asymmetry factor as A_{LR}, caused by the different coupling strengths of the Z^0 to left- and right-handed fermions, and a general cross-section for the sign of polarisation as $\sigma_{i,j}$ where i, j describe the sign of the polarisation, one can write

$$A_{LR} = \frac{\sigma_{LR} - \sigma_{RL}}{\sigma_{LR} + \sigma_{RL}} \tag{2}$$

and

$$\sigma_{i,j} = \frac{1}{4}\sigma_u[1 - \mathcal{P}_{e^-}\mathcal{P}_{e^+} + A_{LR}(\mathcal{P}_{e^-} - \mathcal{P}_{e^+})]. \tag{3}$$

Here, the polarisations are restricted by $|\mathcal{P}| < 1$ for realistic beam values and σ_u is the unpolarised cross-section defined by

$$\sigma_u = \frac{1}{4}[\sigma_{+-} + \sigma_{-+} + \sigma_{--} + \sigma_{++}]. \tag{4}$$

From equation 3 one can see that the σ_{++} and σ_{--}, with $J = 0$, are equal to zero for $\mathcal{P}_{e^-} = \mathcal{P}_{e^+} = \pm 1$. However, for opposite polarisation signs with $J = 1$, the cross-sections are non-zero for $\mathcal{P}_{e^-} = -\mathcal{P}_{e^+} = \pm 1$. It is also possible to show that, by substituting 2 and 4 into 3, one will get back equation 1.

By using the fact that σ_u can be defined in terms of the number of events, N_u, divided by the luminosity, $\mathcal{L}$, and equating this to equation 4, an equation for the effective beam luminosity can be obtained (by following the arguments and steps in reference [7]) and can be written as

$$\frac{\mathcal{L}_{\text{eff}}}{\mathcal{L}} = 1 - \mathcal{P}_{e^+}\mathcal{P}_{e^-}. \tag{5}$$

The ILC will be able to easily obtain an electron beam polarisation of $|\mathcal{P}_{e^-}| = 0.8$. The difficulty comes with the positron source. Currently, a positron beam polarisation of $|\mathcal{P}_{e^+}| = 0.3$ is achievable. With this, there can be an effective luminosity increase of 24%. Although an upgrade that will give a positron beam polarisation of 0.6 could be possible. This would mean an increase of effective luminosity by 48%. This is dependent on the parameters and capability of the helical undulator [6].

2.2 Photon-Matter Interactions

Incoming photons on the titanium alloy target can interact with the wheel in more than one way. This is shown in figure 3 with the total relative probability of several interactions plotted against incoming photon energy. For incoming photons of energy 10 MeV, it can be seen that this is the region where pair production begins to take over as the dominant process.

This plot is a general curve. In reality the total probability of interaction is a function of the atomic number, Z. Each interaction cross-section has an independent contribution to the overall probability. One feature that is not shown in this plot is the energy absorption of a photon in the atomic energy levels. These are called K-edges for x-rays as they are absorbed in the K-band [8]. For example, in titanium the K-edge occurs at approximately 4.96 keV [9].

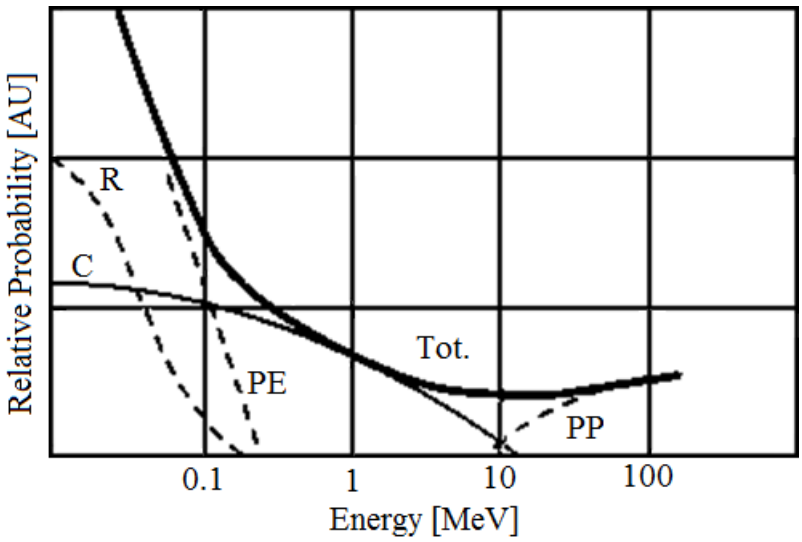

Figure 3: The relative probabilities of Compton, Rayleigh, photoelectric or pair production interactions occurring against incoming photon energy for an arbitrary atomic element.

2.3 Beam Parameters

The incoming electron beam, as it enters the helical undulator, is not continuous. It is split into beam trains that occur approximately 200 ms apart. The duration of a single train is 0.97 ms. Each train is split up further into 2,625 electron bunches and each bunch contains 2×10^{10} electrons in it. Figure 4 best illustrates the time spacing of the beam trains and bunches [10].

The trains have a frequency of 5 Hz. This is to minimise the heat load on the other components in the accelerator. This method of a pulsed beam structure is standard through most particle accelerators. The polarised photon and positron beams will have an identical time structure to the electron beam.

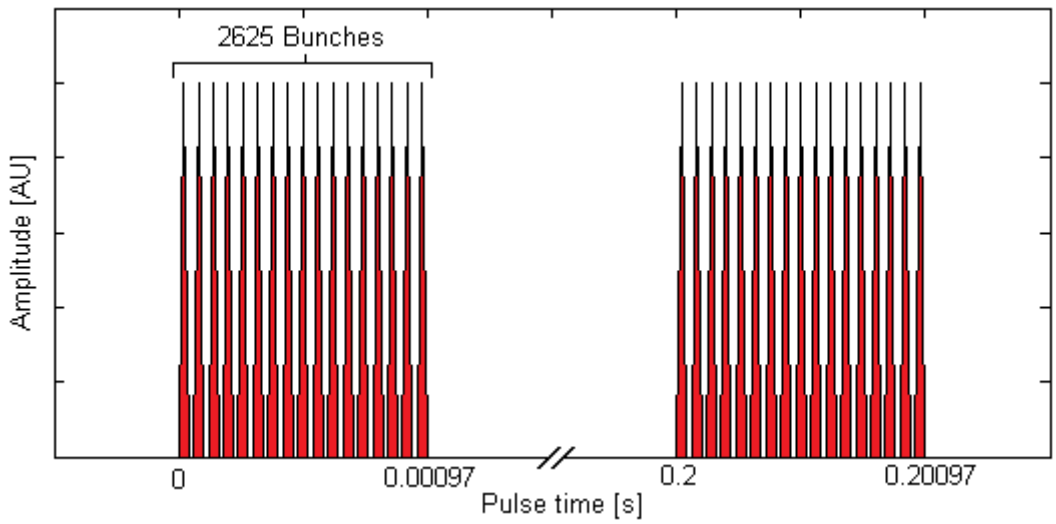

Figure 4: Beam amplitude dependency on time. Each beam train contains 2,625 bunches consisting of $2{\times}10^{10}$ electrons per bunch for a high luminosity.

3 Simulations

All the physical simulations were carried out and computed using the ANSYS software [11]. This software employs the finite element method that uses variational calculus to minimise any error function at the element boundaries. Both target designs were modelled using this software. The designs were simulated for their structural integrities under the forces a heat loads from the photon beam at the rim. Fluid flow was also simulated for the cooling channels that pass through the spokes of the wheel.

3.1 Large Design

Shown in figure 5 is the first design for a positron source target for the ILC. It is made from a Ti(6%)Al(4%)V alloy because of its tensile strength and high melting point. Such an alloy is ideal for electron-positron pair-production at the photon beam energy. The

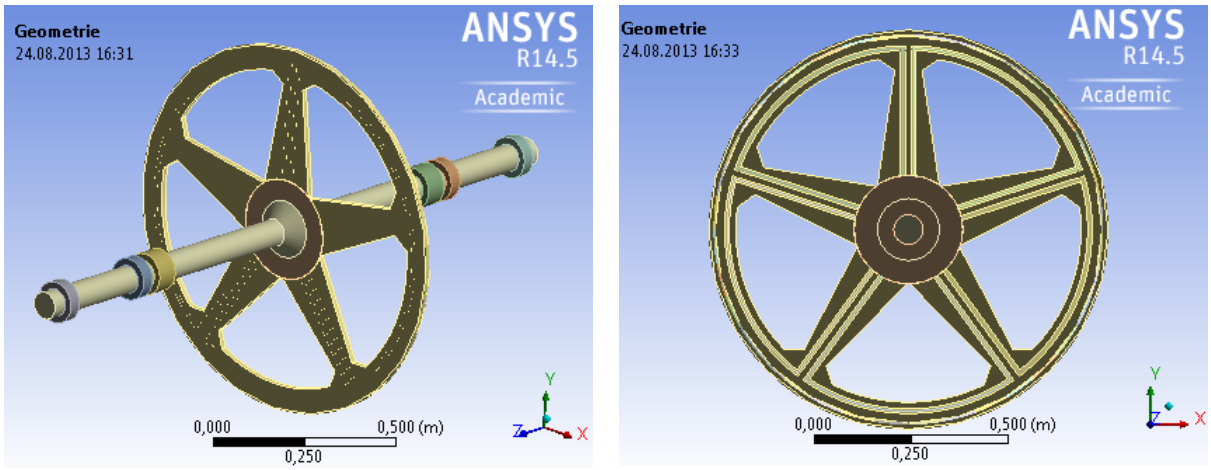

Figure 5: Left: The whole target and axle, the wheel is 1 m in diameter. Right: The cooling channels in the spokes of the wheel.

wheel has a thickness of 1.5 cm, approximately equivalent to 0.4 radiation lengths. It is designed to rotate at a maximum of 2,000 rpm with a diameter of 1 m. This large radius gives the wheel a large moment of inertia. Mathematically, the inertia scales with radius with the relationship

$$I = \sum_{i=1}^{N} m_i r_i^2. \tag{6}$$

This could be a disadvantage to the design, as with this larger inertia, more rotational energy is required to rotate at the necessary angular velocity. Also, a larger radius means that the torque that the rim will experience due to the pressure exerted by the beam will also be greater and will be more likely to cause significant deformation at the rim of the wheel, thus shortening its life-span.

Also shown in figure 5 is a cross-section of the wheel showing internal cooling channels. This allows thermal energy from the beam to be dissipated for efficiently within the target. The channel shape is a square prism with sides of 1.2 cm and the closest approach of one channel to another is 1.6 cm. In ANSYS, the water is simulated using the assumption of lamina flow and therefore does not exhibit any non-linear behaviour that might be present at turning points in the cooling channels, such as turbulence. Although the simulation model does not show this, the real design will carry the water in through the axle from one direction and out of it through the another.

3.2 Small Design

This smaller design was created as an improvement for the more massive and larger design. This includes reducing the radius of the wheel from 50 cm down to 30 cm. This decreases the moment of inertia (as described by equation 6) of the wheel and therefore the energy necessary to rotate it. The axle and the bearing have no alterations to their shape or dimensions. This is shown in figure 6.

To maintain a constant arc distance away from each beam collision point, the rotational velocity was reduced to 1,000 rpm. This causes the rim of the wheel to heat up quicker for each rotation. Therefore, the cooling channels were placed closer to the beam point at a distance of 1 cm. This is also shown in figure 6. This still does not interfere with the emittance of the beam as the spot size is 1.7 mm. As with the larger design, the water is simulated using lamina flow in this smaller model.

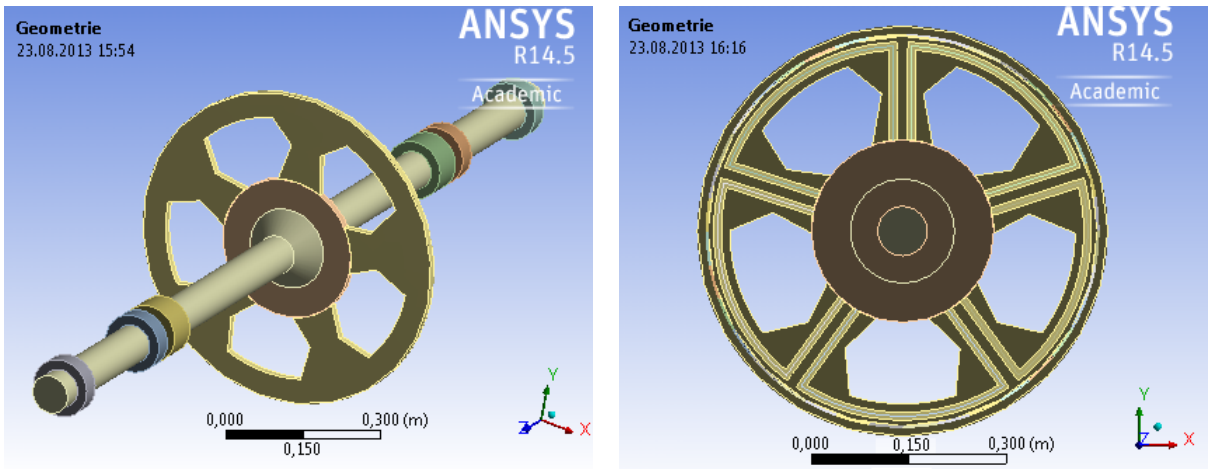

Figure 6: Left: The whole target and axle. This design has a smaller radius than the previous. Right: The cooling channels in the wheel. The thickness of which are unchanged.

4 Results

4.1 Temperature Distribution

Below in figure 7 is a mapping of the temperature distribution of the titanium alloy target. The simulation initial conditions were that the entire wheel was in thermal equilibrium at 20°C. After a 60 s simulation time, the maximum temperature of the wheel reached 252.89°C, well below the temperature at which titanium will start to significantly deform. Most of the thermal energy is focused at the rim of the wheel by design as this is where the photon beam hits the target. From there, the temperature is rapidly decreased due to the addition of cooling channels.

One can see the heat being carried away by the water flow in the cooling channels. The change in temperature of the water throughout the entire process is approximately 1.5°C; ΔT is not significant enough to change the state properties of the water during the process. The cooling channels are 1 cm away from the point at which the beam hits the target. Initial simulations had them at 2 mm but the temperature at the rim was beyond 600°C, too high for the target.

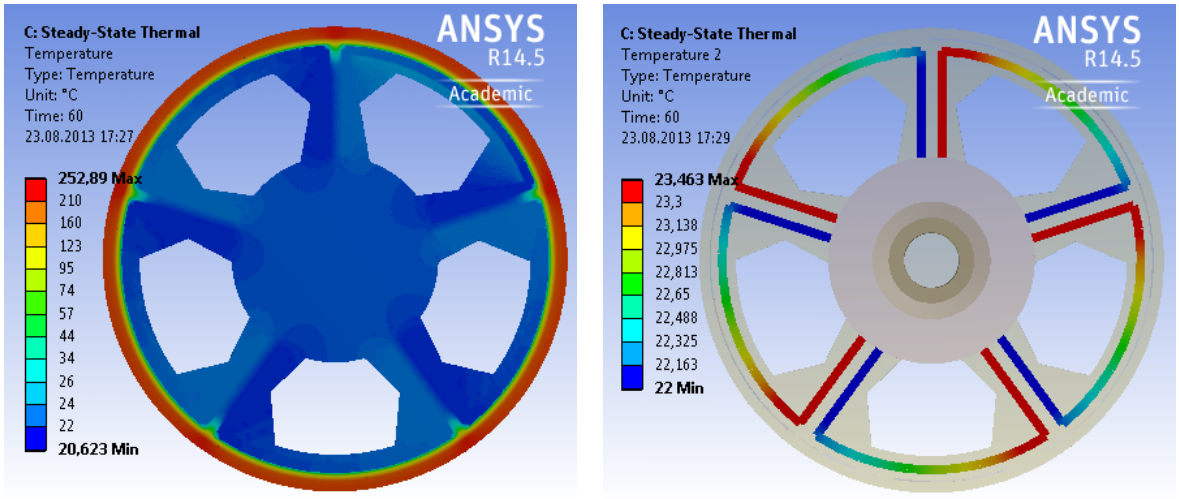

Figure 7: Left: The temperature at the rim of the wheel after repeatedly colliding with the beam. Right: The changing temperature of the water as it cools the rim of the wheel.

4.2 Structural Deformation

The structural deformation of the wheel at its maximum has a displacement of 220 microns radially outwards in the plane of the wheel. This is the point where the spokes are furthest away from the rim of the target. This is an acceptable value and is small enough to be considered negligible to structural integrity. This is best shown in figure 8. The bearings on the axle were modelled as being fixed in the software. Meaning that they are unable to be displaced as they hold the axle in position.

Also shown in figure 8 is an internal cross-section of the wheel. This shows that the cooling channels displayed little to no distortion in their shape and therefore did not affect the water. The water is shown to have zero deformation as it is modelled as a separate body from the rest of the target.

Not shown in this image is how the incoming pressure of the beam distorted the target in the direction parallel to the axle. This, like at the rim of the wheel, is also a negligible amount due to the presence of the axle bearings.

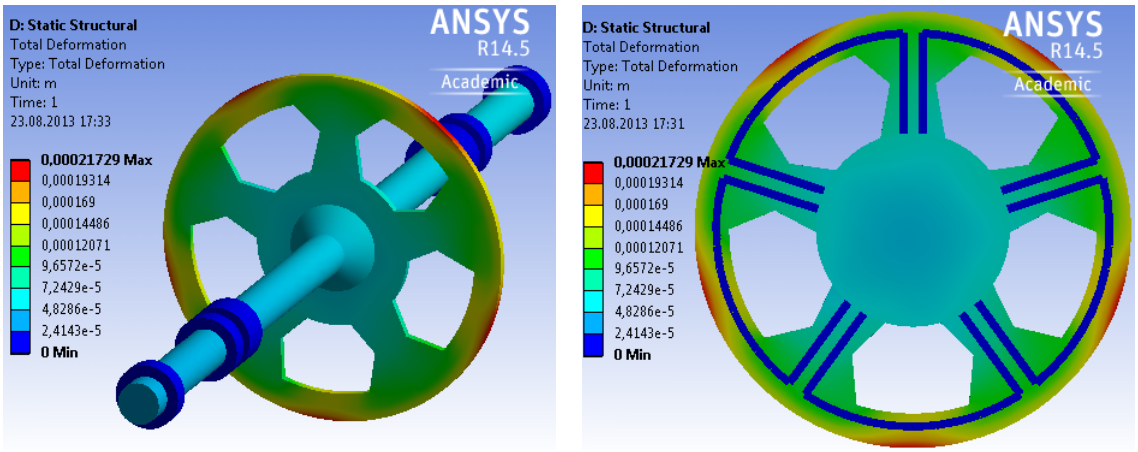

Figure 8: Left: Deformation map of the whole target. The maximum displacement is approximately 220 microns. Right: Cross-section of the wheel. Points equidistant from the spokes are the most deformed.

4.3 Bearing Forces

To establish distinguishability between the six bearings they will be labelled from 'a' to 'f'. This is relative to figure 6 where the purple (apparently closest) bearing is a and the last green (apparently farthest) is f. The rest are labelled in alphabetical order between these two references. As a coordinate system, the axle lies along the z axis with bearing a in the positive z. The target wheel is therefore in the x-y plane.

Below, table 2 shows the individual components of the forces acting on each bearing and the total force. Bearings c and d experience the highest total force out of the six. These are ferrofluid bearings to maintain a vacuum around the target, therefore the pressure difference is greatest on these two. Ferrofluid is chosen as an typical lubricant, such as oil, will not be in the liquid phase at these pressures. These forces are possibly too high for the bearings as they acted on the target for 1 ms. If the target is to have a life-time of two years, these might have to be reduced. Specifically in the x direction. The gap between bearings b and c and also between d and e is the boundary between the vacuum and the surroundings to the target container.

All the force components in the z direction are zero. This is because the simulation modelled the axle in this direction as free. Therefore the axle is allowed to deform in this direction and does so on the order of tens of microns. Again, this is a negligible affect with regards to the structural integrity of the target.

Bearing	F_x (N)	F_y (N)	F_z (N)	F_{tot} (N)
a	34.76	-22.14	0	41.21
b	-30.02	-4.93	0	30.42
c	-133.20	36.15	0	138.02
d	-133.21	20.14	0	134.72
e	-21.89	-6.23	0	22.75
f	26.34	-27.56	0	38.13

Table 2: With reference to figure 6, the closest bearing on the axle is labelled 'a' and the farthest is labelled 'f'. The forces described in the other columns are in units of Newtons.

5 Discussion

The ILC is essential in order to further establish current knowledge in physics and to explore particle physics at a new energy threshold. These goals will be more attainable by having polarised electron and positron beams in the ILC. It is possible to attain an electron beam polarisation of 80% and with the maximum and upgradable possibility of 60% polarised positrons. This is advantageous for increasing apparent beam luminosity and testing predictions made by the SM.

This report introduced two rotating wheel-like positron source targets. Each of a different radius. The design with the smaller radius, therefore smaller mass and inertia, was simulated using the ANSYS software. The results revealed that the temperature change due to an incoming photon beam on the titanium alloy target could be reduced enough that it does not affect the structural integrity of the target. This is because of cooling channels that are at a distance of 1 cm from the beam contact point. The simulation of the targets net deformation, measured as the displacement from the finite elements original position, showed that the maximum value of this was of the order of a few microns. This is also a negligible result from the effects of the beam.

However, the simulations of forces on the bearings show that the initial impact of the photon beam with the target delivers a large force on the bearing in the first few milliseconds of the interaction. This could cause lasting strain that could reduce the two year working life time of the target. A solution to the large initial forces exerted on these bearings would be to model them as elastic, rather than rigid, bodies.

Overall, the smaller target design shows potential as a valid polarised positron source for the ILC. It performs well in dissipating the heat induced by the photon beam in order to minimise damage and deformations of the wheel. Further testing is necessary to observe how much further the wheel could be cooled and to test extra steps to reduce the high impact forces of the photon beam on the target.

Acknowledgements

I would like to thank my supervisors, Friedrich Staufenbiel for his help and tuition in using the ANSYS software and Sabine Riemann resourcefulness in discussions about the physics of polarised beams. I am also thankful to Karl Jansen for organising a successful 2013 DESY summer student programme, the informative lecture schedule and the experience I gained from working and living in Berlin.

References

[1] CERN, 2013. *New results indicate that new particle is a Higgs boson.* CERN. Available from: http://home.web.cern.ch/about/updates/2013/03/new-results-indicate-new-particle-higgs-boson [Accessed 18 August 2013].

[2] Deutsches Elektronen-Synchrotron, 2010. *Particle Physics: Highlights and Annual Report.* Hamburg: Deutsches Elektronen-Synchrotron.

[3] International Linear Collider, 2007. *Reference Design Report: Detectors.* Vol. 4. Chapter 8. Multinational Collaborators: International Linear Collider.

[4] International Linear Collider, 2007. *Reference Design Report: Accelerator.* Vol. 3. Chapter 2. Multinational Collaborators: International Linear Collider.

[5] International Linear Collider, 2013. *Technical Design Report: Executive Summary.* Vol. 1. Chapter 3. Multinational Collaborators: International Linear Collider.

[6] G. A. Moorgat-Pick *et al.*, 2008. *Polarized positrons and electrons at the linear collider.* Physics Reports, 460 (2008) 131-243. Available from: http://www.sciencedirect.com [Accessed 20 August 2013].

[7] S. Riemann, 2011. *Physics Applications of Polarized Positrons* In: W. Gei, ed. *Polarized Positron 2011.* Singapore: World Scientific Publishing, 1-15.

[8] J. Lilley, 2007. *Nuclear Physics: Principles and Applications.* Chichester: John Wiley & Sons Ltd.

[9] J. H. Hubbell and S. M. Seltzer, 1996. *Tables of X-Ray Mass Attenuation Coefficients and Mass Energy-Absorption Coefficients from 1 keV to 20 MeV for Elements Z = 1 to 92 and 48 Additional Substances of Dosimetric Interest.* National Institute of Standards and Technology, Version 1.4. Available from: http://physics.nist.gov/xaamdi [Accessed 21 August 2013].

[10] F. Staufenbiel *et al.*, 2011. *Heat Load and Stress Studies for a Design of the Photon Collimator for the ILC Positron Source* In: W. Gei, ed. *Polarized Positron 2011.* Singapore: World Scientific Publishing, 71-80.

[11] ANSYS, 2013. *Introduction to Engineering Simulation Hands-On Workshops.* ANSYS. Available from: http://www.ansys.com/ukintrosem [Accessed 29 August 2013].